Journal of Luminescence 144 (2013) 45–52

Contents lists available at SciVerse ScienceDirect

Journal of Luminescence

journal homepage: www.elsevier.com/locate/jlumin

On the response of $GdAlO_3$:Ce powder scintillators

C. Michail [a,*], N. Kalyvas [a], I. Valais [a], S. David [a], I. Seferis [b], A. Toutountzis [a], A. Karabotsos [c], P. Liaparinos [a], G. Fountos [a], I. Kandarakis [a]

[a] Department of Medical Instruments Technology, Technological Educational Institute of Athens, 122 10 Athens, Greece
[b] Department of Medical Physics, Medical School, University of Patras, 265 00 Patras, Greece
[c] Department of Conservation of Antiquities and Works of Art, Technological Educational Institute of Athens, 122 10 Athens, Greece

ARTICLE INFO

Article history:
Received 7 February 2013
Received in revised form
18 June 2013
Accepted 27 June 2013
Available online 4 July 2013

Keywords:
Inorganic scintillators
Radiation detectors
$GdAlO_3$:Ce

ABSTRACT

The aim of the present study was to investigate the luminescence efficiency (XLE) of gadolinium aluminum perovskite ($GdAlO_3$:Ce) powder scintillator. This powder phosphor, also known as GAP:Ce scintillator, is a non-hygroscopic material, emitting blue light with short decay time. For the purposes of this study, five scintillating screens with coating thicknesses, 14.7, 31.0, 53.7, 67.2 and 121.1 mg/cm^2, were prepared in our laboratory from $GdAlO_3$:Ce powder (Phosphor Technology, Ltd) by sedimentation on silica substrates. The light emitted by the phosphors under investigation was evaluated by performing measurements of the absolute luminescence efficiency (AE), X-ray luminescence efficiency and detector quantum gain (DQG) under X-ray exposure conditions with tube voltages ranging from 50 to 140 kV. The quantum detection efficiency (QDE) and energy absorption efficiency (EAE) were also evaluated. The spectral compatibility of $GdAlO_3$:Ce, with various existing optical detectors, was investigated after emission spectra measurements. A theoretical model, describing radiation and light transfer, was used to fit experimental AE data. This has allowed the estimation of optical attenuation coefficients of the scintillator. $GdAlO_3$:Ce exhibited higher QDE and EAE values, compared to aluminium perovskite ($YAlO_3$:Ce) but lower absolute efficiency values. Absolute efficiency was found to increase with increasing X-ray tube voltage, although for values higher than 120 kVp a decrease was observed.

1. Introduction

Most medical imaging detectors are based on scintillator–optical detector (photodiodes, photocathodes, films etc.) combinations. Cerium (Ce^{3+}) doped scintillators or phosphors exhibit the property of very fast response. The latter is dominated by the very efficient 5d→4f electronic transitions in the Ce^{3+} ion [1–4]. Previous studies have shown that yttrium aluminium perovskite ($YAlO_3$:Ce) also known as YAP:Ce has attractive properties [5,6]. On the other hand gadolinium based scintillators (e.g. Gd_2O_2S:Tb) are widely used in X-ray imaging applications. Using gadolinium (Gd) which is heavier than yttrium (*Y*), higher absorption efficiency is expected. In cerium doped gadolinium aluminium perovskite ($GdAlO_3$:Ce also known as GAP) powder scintillator, yttrium has been replaced by gadolinium [7–14]. GAP:Ce has been studied thoroughly in the past [7–18], however, it has never been tested under X-ray radiography conditions. It has been used in electronics as a dielectric layer for flash memory devices [19], as a light converting material substrates for use in light emitting diode (LED) substrates [20] and optical ceramic materials [21,22]. Initial luminescence results were published by our group in the past [7]. In the present study, a systematic investigation of the $GdAlO_3$:Ce was performed. Absolute luminescence efficiency measurements were performed for various X-ray tube voltages (50–140 kVp). Parameters related to X-ray detection such as the energy absorption efficiency (EAE) and the quantum detective efficiency (QDE) were calculated. Emitted spectrum and spectral compatibility to optical sensors were determined by performing light emission spectra measurements and by taking into account the spectral sensitivity of the optical detectors. Quality metrics such as quantum gain (DQG) was estimated. An analytical model was used to predict optical properties of the $GdAlO_3$:Ce scintillator [5,23].

2. Materials and methods

2.1. Calculations

2.1.1. Attenuation coefficients for compounds

Attenuation coefficients for compounds (materials comprised of ≥2 elements) can be determined as the weighted average (by mass) of the individual mass attenuation coefficients of the

* Corresponding author. Tel.: +30 6973436513.
E-mail addresses: michail@upatras.gr, darkthvader80@gmail.com (C. Michail).

0022-2313/$ - see front matter © 2013 Elsevier B.V. All rights reserved.
http://dx.doi.org/10.1016/j.jlumin.2013.06.041

compound's constituent elements, as

$$\left(\frac{\mu}{\rho}\right)_{\text{compound}} = \sum_{i=1}^{N} m_i \left(\frac{\mu}{\rho}\right)_i \quad (2.1)$$

where m_i is the mass fraction (fraction of the element's mass contribution to the total mass) and $(\mu/\rho)_i$ is the mass attenuation coefficient of element i in the compound. This is important for estimating attenuation probabilities of compounds and materials that cannot be easily measured and particularly for computer simulations [24,25].

2.1.2. Quantum detection and energy absorption efficiency (QDE & EAE)

The efficiency of a scintillator to detect photons is conventionally described by the quantum detection efficiency (QDE), which is defined as the fraction of incident photons interacting with the scintillator mass [1]. However accurate X-ray detection may be determined by considering only those X-ray photons that deposit an amount of energy in the phosphor mass. This is because only these X-rays can generate light signals (scintillations) which can may be detected by the optical sensor and contribute to image formation. The fraction of energy depositing photons is expressed through the energy absorption efficiency (EAE). QDE as well as EAE were evaluated analytically [1] as described in previous studies [26]. The required values for the total attenuation and the total energy absorption coefficients of $GdAlO_3$:Ce scintillator were calculated from tabulated data of energy absorption and attenuation coefficients of gadolinium, aluminum and oxygen [27,28].

2.2. Experiments

$GdAlO_3$:Ce was purchased in powder form (Phosphor Technology Ltd, England, code: UM58#9438) with a mean grain size (estimated by ultrasonic dispersion with a coulter counter having 100 μm aperture) of approximately 8.9 μm at the 95% of the volume and quartile deviation of 0.32 (Phosphor Technology Ltd., datasheet). $GdAlO_3$:Ce has $Z_{eff} = 56.2$, refractive index=2.02 [21] and a very fast decay time of the order of a few ns [29]. The forbidden energy band-gap between the valence and the conduction energy bands of the $GdAlO_3$:Ce scintillator material is $E_g = 5$ eV [2,3,30,31].

Particle size and morphology parameters of the $GdAlO_3$:Ce powder phosphor were verified via scanning electron microscope (SEM) micrographs using the Jeol JSM 5310 scanning electron microscope (SEM) collaborating with the INCA software. Gold was used to obtain a figure from a site of interest of the $GdAlO_3$:Ce specimen. For the elementary particle analysis carbon thread evaporation process was used. Carbon was flash evaporated under vacuum conditions to produce a film suited for the $GdAlO_3$:Ce SEM specimen in a BAL-TEC CED 030 carbon evaporator (~10^{-2} mbar). The phosphor was used in the form of thin layers to simulate the intensifying screens employed in X-ray imaging. Five screens from 14.7 to 121.1 mg/cm^2 thick were prepared by sedimentation of $GdAlO_3$:Ce powder on fused silica substrates (spectrosil B). The screen coating thicknesses correspond to thicknesses calculated thicknesses of 39.2, 82.67, 143.2, 179.2 and 322.9 μm assuming a density of 7.5 g/cm^3 and a packing density of 50% [5,17]. Sodium orthosilicate (Na_2SiO_3) was used as binding material between the powder grains [26].

The effect of the fused silica substrates (spectrosil B) on the emitted light of the $GdAlO_3$:Ce powder phosphors was also investigated by transmission and absorption measurements. The purpose of these measurements was to confirm that the emission wavelength of the phosphors does not influence drastically the absorption and scattering properties of the substrate. The transmission measurement was carried out with a Perkin-Elmer Lambda 15 UV/vis spectrophotometer.

The phosphor screens were exposed to X-rays on a Philips Optimus radiographic unit, with a dual-focus rotating tungsten anode, employing X-ray tube voltages ranging from 50 to 140 kVp. Tube filtration was 2.5 mm Al. An additional 20 mm filtration was introduced in the beam to simulate beam quality alternation by a human body [32].

2.2.1. Absolute efficiency (AE)

The light emission efficiency of a phosphor may be experimentally estimated under X-ray imaging conditions, by determining the absolute luminescence efficiency (AE) defined by Eq. (2.2):

$$\eta_A = \dot{\Psi}_\lambda / \dot{X} \quad (2.2)$$

where $\dot{\Psi}\lambda$ is the emitted light energy flux (energy of light per unit of area and time), $\dot{X}$ is the incident exposure rate that excites the phosphor to luminescence. AE, is traditionally expressed, in units of $\mu W \times m^{-2}/(mR \times s^{-1})$ thereafter referred to as efficiency units (E.U.). The S.I. equivalent of this unit is given in $\mu W \times m^{-2}/(mGy \times s^{-1})$, where mGy stands for the corresponding air Kerma. The light flux measurements were performed using an experimental set up comprising a light integration sphere (Oriel 70451) coupled to a photomultiplier (PMT) (EMI 9798B) which was

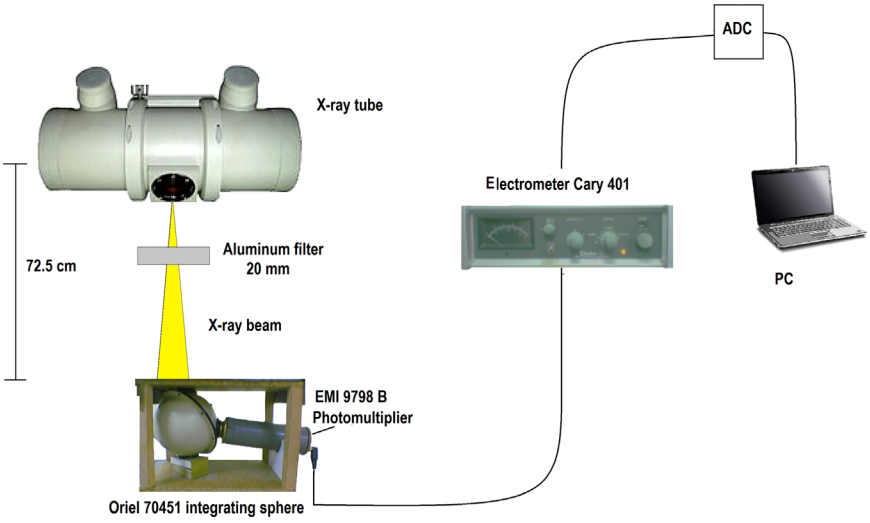

Fig. 1. Experimental set-up for the measurement of the emitted light energy flux comprising the integrating sphere, the PMT and the vibrating reed electrometer.

connected to a Cary 401 vibrating reed electrometer. The photomultiplier was coupled to the output port of the integrating sphere in order to reduce experimental errors due to illumination no uniformities. The screen was positioned at the input port of the integrating sphere whereas the photomultiplier was adapted at the output port (Fig. 1). The photocathode of the photomultiplier (extended S-20) was directly connected to a Cary 401 vibrating reed electrometer by bypassing all dynodes. In this manner, photocurrent instability and electronic noise amplification due to photomultiplier's dynode high voltage were avoided [33].

The light flux of the screens was finally determined after corrections on the experimental data according to the following formula [34]:

$$\dot{\Psi}_{\Lambda} = \frac{I_{elec}}{\tau_0(s_{PC}a_s)} \times \frac{1}{A_{sc}} \tag{2.3}$$

I_{elec} is the current at the output of the electrometer (in pA), s_{PC} is the peak photosensitivity of the photocathode (in pA/W), which was used as a factor converting the output photocathode current into light energy flux. a_s is the spectral matching factor of the screen's emission spectrum to the spectral sensitivity of the photocathode (extended S-20) used to correct for the spectral mismatches between the emitted light and the spectral sensitivity of the photocathode (extended S-20) of the photomultiplier (see Section 2.2.2). A_{sc} is the irradiated area of the screen.τ_0 denotes the throughput of the integration sphere, which is expressed by the ratio (Oriel 70451 integrating sphere data sheet) [35,36]:

$$\tau_0 = \frac{\Psi_e}{\Psi_i} = \frac{\rho_o A_e/A_{sc}}{(1-\rho_o(1-A_p/A_{sc}))} \tag{2.4}$$

Ψ_e is the total light flux at the exit (output) port of the integrating sphere, Ψ_i is the total flux at the input port, A_e is the area of the exit port, A_p is the sum of all port areas and ρ_o denotes the reflectance of the internal sphere wall. Using the setup of Fig. 1 and prototype light emitting diodes (LED, Kingbright Company), the total throughput of the apparatus was calculated, by taking also into account specific data (on A_e, A_{SC}, A_p,ρ_o) given by the manufacturer's datasheet. The calculated throughput value was then $\tau_0 = 15.6$ [34].

2.2.2. Effective efficiency (ηeff)

Since scintillators and phosphor screens are always used in combination with photodetectors (radiographic films, photodiodes, photocathodes etc.), an estimation of the emitted light spectrum compatibility with the spectral sensitivity of photodetectors is required. This compatibility is often expressed by the spectral matching factor αs, which can be calculated as:

$$\alpha s = \int \phi\lambda(\lambda) SD(\lambda) d\lambda / \int \phi\lambda(\lambda) d\lambda \tag{2.5}$$

where $\phi\lambda(\lambda)$ is the emitted light spectrum of the phosphor and $SD(\lambda)$ is the normalized spectral sensitivity distribution of the photodetector used with the phosphor. The spectral matching factor, expresses the spectral compatibility of the phosphor's spectrum with respect to the photodetector [37].

The effective efficiency (ηeff) has been defined [32] by Eq. (2.6):

$$neff = \eta_A \times \alpha s \tag{2.6}$$

The mean light photon energy $E\lambda$ and the spectral matching factor αs, were determined from the emitted light spectrum of the $GdAlO_3$:Ce powder phosphors. The spectral sensitivities of the optical detectors were obtained from manufacturers' data.

2.2.3. X-ray luminescence efficiency (XLE)

The efficiency of a scintillating screen to transfer the signal from the input to the output is expressed by the X-ray luminescence efficiency (*XLE*). *XLE* is defined as the ratio of the emitted light energy fluence over the incident X-ray energy fluence: ($\eta_\psi = \Psi_\Lambda/\Psi_0$).

The X-ray luminescence efficiency η_ψ was determined by performing X-ray exposure and emitted light energy flux measurements. Ψ_Λ measurements were performed using the experimental setup described in Section 2.2.1 [32]. For the calculation of XLE, the X-ray energy flux, Ψ_0 in Eq. (2.4), was determined by converting X-ray exposure data X [32] as follows: $\Psi_0 = X\hat{\Psi}$ where $\hat{\Psi}$ is a function defined as the X-ray energy flux per exposure rate, which may be estimated as follows:

$$\hat{\Psi} = \int \Psi_0(E)dE / \left(\int \Psi_0(E)\left[X/\Psi_0(E)\right]dE \right) \tag{2.7}$$

where

$$X/\Psi_0(E) = (\mu_{en}(E)/\rho)_{\text{air}} \times (W_A/e)^{-1} \tag{2.8}$$

is the factor converting energy flux into exposure rate, $(\mu_{en}/\rho)_{\text{air}}$ is the X-ray mass energy absorption coefficient of air at energy E, and (W_A/e) is the average energy per unit of charge required to produce an electron-ion pair in air. The values of (W_A/e) and $(\mu_{en}/\rho)_{\text{air}}$ were obtained from the literature [27].

2.2.4. Detector quantum optical gain (DQG)

Detector quantum optical gain (DQG) was determined according to the ratio Φ_Λ/Φ_X, where the Φ_X is the X-ray photon flux. The emitted light photon fluence, may be expressed in terms of experimentally measurable quantities (absolute efficiency, exposure, mean light wavelength) by using Eq. (2.9):

$$\Phi_\Lambda = \Psi_\Lambda / hc\bar{\lambda}^{-1} \tag{2.9}$$

where $hc/\bar{\lambda}$ is the average energy of emitted light photons ($E_\lambda = hc/\bar{\lambda}$), $\bar{\lambda}$ being the mean light wavelength determined from emission spectra measurements [26] as follows:

$$hc\bar{\lambda}^{-1} = hc\left\{ \int \phi_\Lambda(\lambda)\lambda d\lambda / \int \phi_\Lambda(\lambda) d\lambda \right\}^{-1} \tag{2.10}$$

where $\phi_\Lambda(\lambda)$ is the measured scintillator emission spectrum [26].Φ_X was determined by using Eqs. (2.7) and (2.8) and replacing Ψ_0 by Φ_0 and dividing Eq. (2.8) by the X-ray energy [32]:

2.3. Analytical modeling

2.3.1. Absolute luminescence efficiency (AE)

The efficiency of the phosphor light output is affected by the intrinsic physical processes that occur within the screen. The contribution of these intrinsic processes can be expressed by the Absolute Luminescence Efficiency in which the light propagation within a phosphor screen can be described by a one-dimensional radiation transfer model [5]:

$$AE = \frac{n_C\gamma(E)t_r\mu(E)(1+\rho)e^{-\mu(E)T}}{2(\mu(E)^2-\sigma^2)} \frac{(\mu(E)-\sigma)(1-\beta)e^{-\sigma T} + 2(\sigma+\mu(E)\beta)e^{\mu(E)T} - (\mu(E)+\sigma)(1+\beta)e^{\sigma T}}{(1+\beta)(\rho+\beta)e^{\sigma T} - (1-\beta)(\rho-\beta)e^{-\sigma T}} \tag{2.11}$$

where,$\mu(E)$is the X-ray energy mass absorption coefficient for X-ray energy E, $\gamma(E)$ is a conversion factor converting energy fluence (W/m^2) into exposure rate (mR/s), t_r is the transparency of the phosphor screen substrate and T is the thickness (surface density) of the scintillator and σ,β and ρ are optical parameters related to light absorption, light scattering and light reflectivity in the phosphor material [38].

If the energy spectrum of X-rays,$f(E)$, is to be taken into account, then AE can be calculated by summing over this spectrum, up to the peak energy (kVp) of the X-ray spectrum:

$$AE_{kVp} = \sum_E f(E)AE / \sum_E f(E) \tag{2.12}$$

where kVp denotes the high voltage (kilovolt peak) applied to the X-ray tube. This voltage is equal to the maximum energy of the X-ray spectrum, expressed in KeV.

In order to theoretically investigate the response of $GdAlO_3$:Ce and determine the parameters related to optical photon propagation to the output, Eqs. (2.11) and (2.12) was used to fit the experimental data. The fitting was performed by first selecting values for the parameters, ρ and β ($\rho=0.90$ and $\beta=0.03$) from our previous studies [38]. The value of t_r was set equal to 0.807, (calculated from the Fresnel equations) assuming normal light incidence, where the index of refraction of the optical silica substrate was taken equal to 1.48, at approximately 342 nm [39]. σ and n_C were fitted to the experimental data for an X-ray spectrum of 70 kVp, filtered by 20 mm Al. The X-ray spectrum that was used for the AE calculation with Eq. (2.12) was obtained from direct X-ray spectra measurement with a portable cadmium telluride (CdTe) detector [23,40].

3. Results and discussion

Fig. 2 shows the calculated mass energy absorption and attenuation coefficients for the $GdAlO_3$:Ce and $YAlO_3$:Ce phosphors. The values of the energy absorption coefficients were calculated from tabulated data on absorption coefficients.

Figs. 3 and 4 illustrate the variation of calculated QDE and EAE with X-ray tube voltage for the screens, with coating thicknesses of 14.7, 31.0, 53.7, 67.2 and 121.1 mg/cm^2. As it can be seen the quantum detection efficiency values are higher than the energy absorption efficiency ones. This can be explained by the fact that EAE does not include the effect of scattered, *K* or *L*-fluorescence, and bremsstrahlung radiations while QDE expresses all the mechanisms of X-ray quanta interaction within the phosphor. Energy absorption efficiency value at 80 kVp for $GdAlO_3$:Ce for 121.1 mg/cm^2 screen was found at 0.275. For comparison purposes similar calculations were performed for a 67.2 mg/cm^2 coating thickness $YAlO_3$:Ce screen. For energies higher than 60 kVp QDE of the $GdAlO_3$:Ce screen is clearly higher than the corresponding values of $YAlO_3$:Ce with the same screen thickness (Fig. 3a). Furthermore the 67.2 mg/cm^2 $GdAlO_3$:Ce exhibits higher EAE values than the corresponding $YAlO_3$:Ce across the X-ray tube voltage range (Fig. 4a). This can be explained by the presence of gadolinium which is heavier than yttrium.

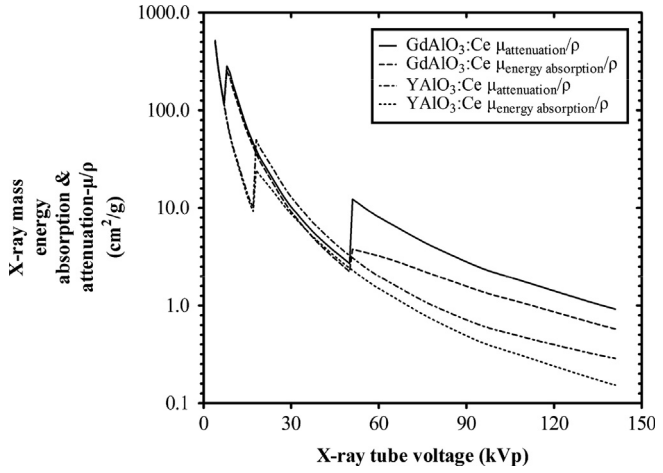

Fig. 2. Calculated X-ray mass energy absorption and attenuation coefficients of the $GdAlO_3$:Ce and $YAlO_3$:Ce phosphors calculated with the XMuDat photon attenuation data version 1.0.1 software, data source J H Hubbell, S M Seltzer, NISTIR 5632, 1995 [27].

Qualitatively the particle sizes of $GdAlO_3$:Ce phosphor has a mean grain size of 8.9 μm (obtained from Phosphor Technology Ltd, England, code: UM58#9438 data sheet). A fragment image of $GdAlO_3$:Ce powder phosphor is presented in Fig. 5. It was shown by energy dispersive X-ray (EDX) that the powder is really $GdAlO_3$:Ce with no admixtures. Normalized stoichiometric results, obtained by the SEM on the region of interest (ROI) of Fig. 5, showed the following % weights of the elements in the mixture: Gadolinium (Gd) 71.07%, oxygen (O) 19.25%, aluminum (Al) 8.61% and cerium (Ce) 1.06%.

Fig. 6 shows that in the 330 to 354 nm wavelength range ($GdAlO_3$:Ce emission wavelength) the transparency of the substrate is 92.35%. This finding reveals that the emission wavelength would not be influenced drastically by the reflection and scatter properties of the substrate.

Fig. 7 shows the variation of absolute luminescence efficiency of the $GdAlO_3$:Ce screen with X-ray tube voltage in the range from 50 to 140 kVp. Points represent experimental data. AE was found to increase for all screens continuously with increasing X-ray tube voltage up to 100 kVp. For higher X-ray tube voltages AE showed a tendency to saturate (110 to 120 kVp) and decrease thereafter. An important observation is that absolute efficiency maintains high values within a range of X-ray tube voltages from 100 to 120 kVp. However these values are lower than the corresponding values of $YAlO_3$:Ce screens that were measured in a previous study of our group [5]. The low absolute efficiency values of the $GdAlO_3$:Ce can be attributed to a second absorption band in the ultraviolet, next to the 4f-5d absorption of Ce^{3+} which occurs up to the Ce^{3+} emission transition and this absorption will therefore restrict the efficiency of the Ce^{3+} emission, independent of the excitation source [14]. The highest absolute efficiency values were observed for the 67.2 mg/cm^2 screen. This finding shows that adequate efficiency can be also achieved with lower coating thickness.

Fig. 8 shows the emitted optical spectrum of $GdAlO_3$:Ce normalized to unity and the normalized spectral sensitivity distribution functions of various commonly employed optical photon detectors; the actual sensitivity distributions of optical detectors cover a much wider wavelength region than the small portion of interest shown.

In the $GdAlO_3$:Ce spectrum, the typical $5d \rightarrow 4f$ Ce^{3+} [$^2F_{5/2}$, $^2F_{7/2}$] doublet emission can be observed, which consists roughly of two Gaussian bands with maxima at 330 and 354 nm, lying in the blue region of the optical spectrum [11]. The spectrum of $GdAlO_3$:Ce is narrow enough to assure very good spectral compatibility with the spectral sensitivities of many optical detectors.

Table 1 shows the values of the spectral matching factors of the $GdAlO_3$:Ce, calculated according to relation Eq. (2.2). The optical detectors listed are frequently used in various digital imaging applications, namely: (i) amorphous hydrogenated silicon photodiode (a-Si:H), employed in photodiodes and thin film transistors of modern active matrix flat panel radiographic and fluoroscopic detectors, (ii) GaAs and E/S 20 photocathodes incorporated in various types of fluoroscopic image intensifiers and in photomultipliers, (iii) crystalline silicon (Si) employed in photodiodes, (iv) CCD sensor arrays used in digital radiography and digital mammography systems, (v) avalanche photodiodes (APD) and films used in conventional radiography and mammography (Fuzi UM and Agfa Mammoray). $GdAlO_3$:Ce exhibits excellent compatibility with the Fuzi UM film (1.00) and very good compatibility with photocathodes, such as the GaAs (0.90), the extended S20 (0.82) and the S-9 (0.72). Also it has good compatibility with CCD S100AB (0.89) and the Agfa Mammoray film (0.65). It exhibits moderate compatibility with wavelength selective photodiode, such as the WS-7 A1 (0.45), avalanche photodiodes such as the Hamamatsu S5343 with a gain of 50 (0.31) and amorphous hydrogenated silicon

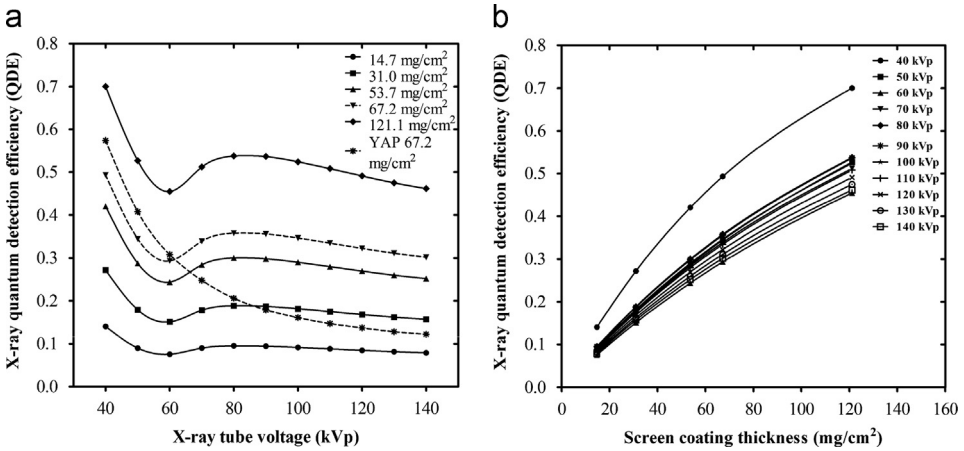

Fig. 3. Variation of the calculated QDE for $GdAlO_3$:Ce powder screens (a) with X-ray tube voltage and comparison with $YAlO_3$:Ce powder screens (b) with screen coating thickness of the $GdAlO_3$:Ce powder screens.

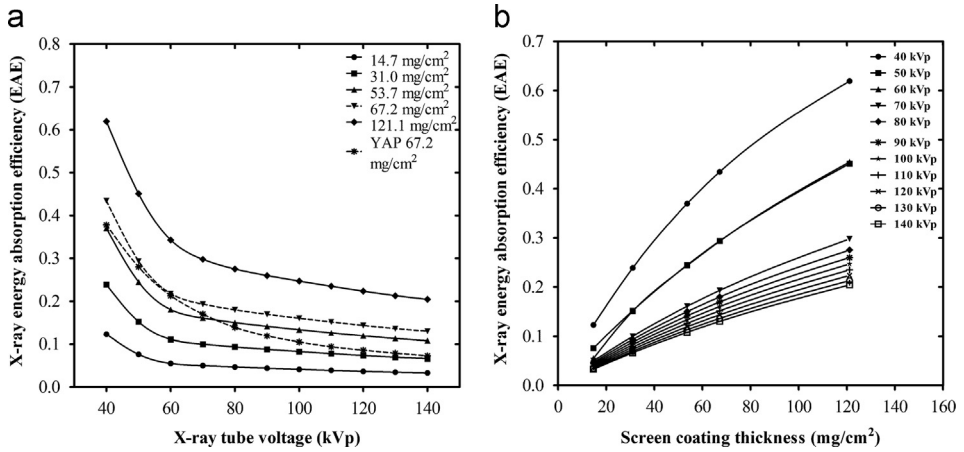

Fig. 4. Variation of the calculated EAE for $GdAlO_3$:Ce powder screens (a) with X-ray tube voltage and comparison with $YAlO_3$:Ce powder screens (b) with screen coating thickness of the $GdAlO_3$:Ce powder screens.

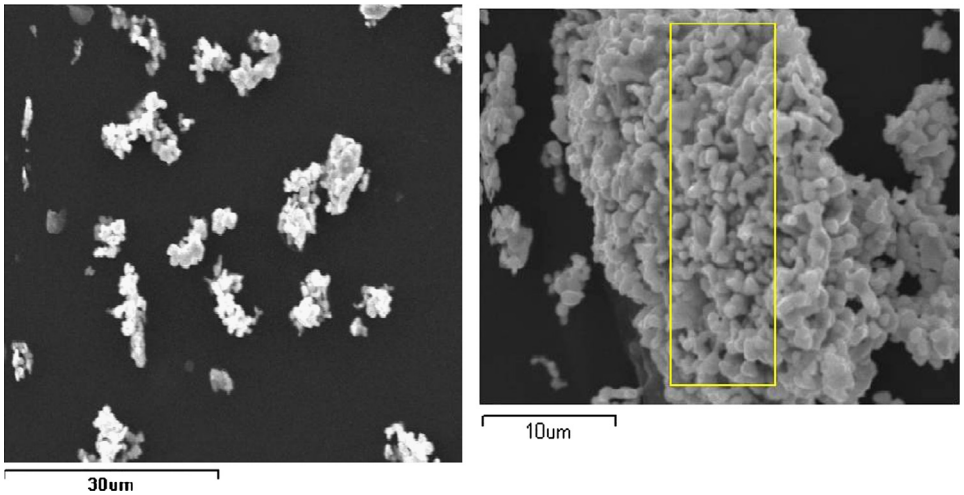

Fig. 5. Scanning electron microscope (SEM) images from a site of interest of the $GdAlO_3$:Ce phosphor.

photodiode (0.35). In addition, it was found incompatible with the silicon (Si) photodiode detectors (0.09). The moderate spectral sensitivity with digital sensors can be explained by the following. In X-ray imaging applications, the converter screen can be directly coupled to the photo detector [23] or indirectly coupled by an optical relay (lens, fiber optic taper, etc.). The latter solution is suffering of a very low transmission below 400 nm. In addition, only few and expensive modern 2D imaging CCD or CMOS imaging sensors, based on crystalline silicon (Si), are sensitive below 400 nm. In this work however, the optical properties of the fused silica substrates, used in the case of the test screens under investigation, does not change in the wavelengths below 400 nm. Data of spectral

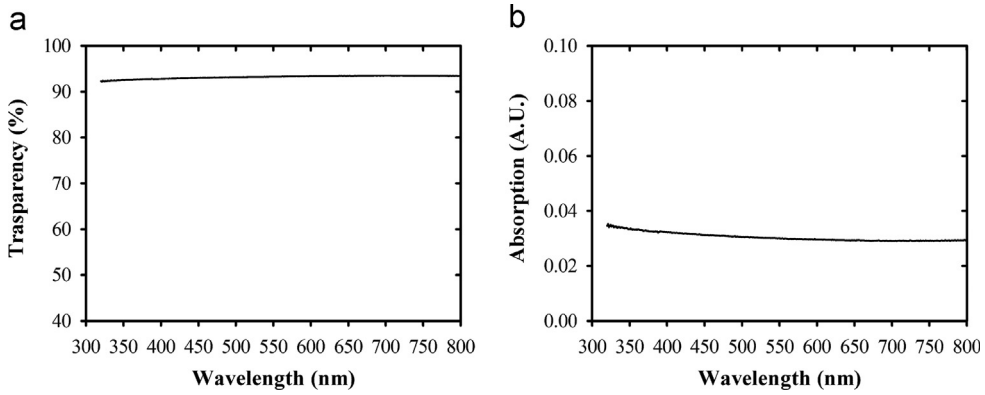

Fig. 6. (a) Optical transmission and (b) absorption measurements of the fused silica substrate (Spectrosil B).

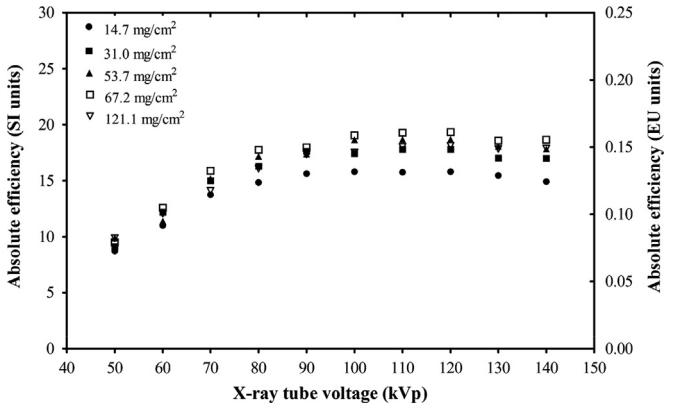

Fig. 7. Absolute luminescence efficiency of the GAP:Ce powder phosphor with X-ray tube voltage for various coating thicknesses. Points correspond to experimental values. Efficiency units (E.U.S.I.): $\mu W \times m^{-2}/(mR \times s^{-1})$ ($\mu W \times s/mGy \times m^2$).

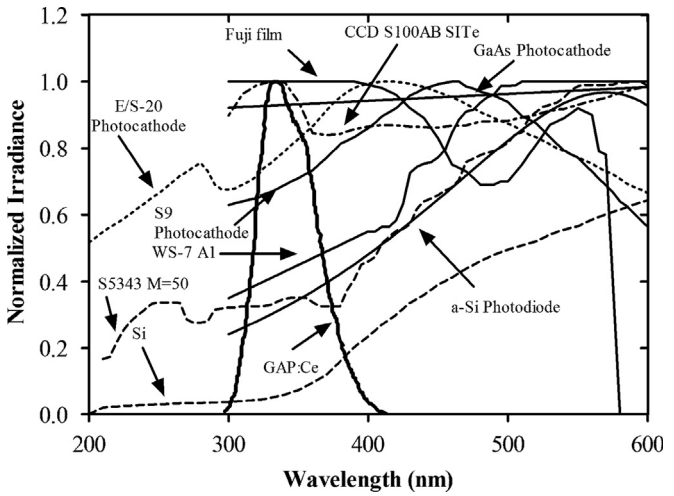

Fig. 8. Normalized emitted light spectrum of $GdAlO_3$:Ce scintillator and spectral sensitivity of various light detectors.

matching factors indicate that $GdAlO_3$:Ce powder phosphor may be adequate coupled to various practical types of digital and analogue optical photon detectors, except crystalline silicon (Si) based photodiodes, which showed low matching factor (0.09).

Fig. 9 shows the effective luminescence efficiency of the 67.2 mg/cm^2 $GdAlO_3$:Ce phosphor scintillator with various analogue and digital optical detectors. All effective efficiency values spread from the absolute efficiency ones, due to the variety of the spectral matching of the light emitted by the $GdAlO_3$:Ce phosphor

Table 1
Spectral matching factors.

Optical detectors	$GdAlO_3$:Ce
Mammoray film	0.65
Fuzi UM film	1.00
Extended S20 Photocathode	0.82
S-9 Photocathode	0.72
GaAs Photocathode	0.90
CCD S100AB SITe	0.86
APD Hamamatsu S5343 $M=50$	0.31
Wavelength selective Photodiode WS-7 A1	0.45
a-Si Photodiode	0.35
Si Photodiode	0.09

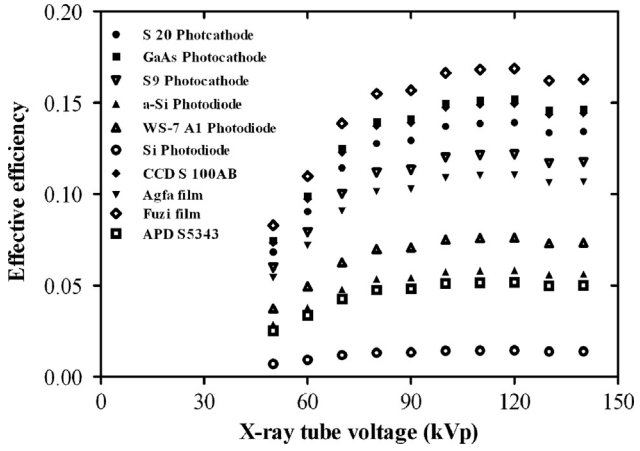

Fig. 9. Effective efficiency of the 67.2 mg/cm^2 $GdAlO_3$:Ce scintillator combined with various photodetectors.

to the various photodetectors. The best effective luminescence efficiency was found for the Fuzi UM film (Matching Factor 1) and the worst for the crystalline silicon (Si).

Fig. 10 shows the X-ray luminescence efficiency (XLE) for the $GdAlO_3$:Ce phosphor screens for various tube voltages. A first point to make is that, neglecting the XLE values in the 50 to 70 kVp X-ray tube voltage range, a tendency of the XLE to decrease with increasing tube voltage is clearly shown. The main reason governing this behaviour should be attributed to the energy absorption properties of the phosphor. However the shape of the XLE curves should be additionally affected by the light transmission through the screen. As X-rays penetrate deeper in the phosphor mass, at higher voltages, light photons are created closer to the screen

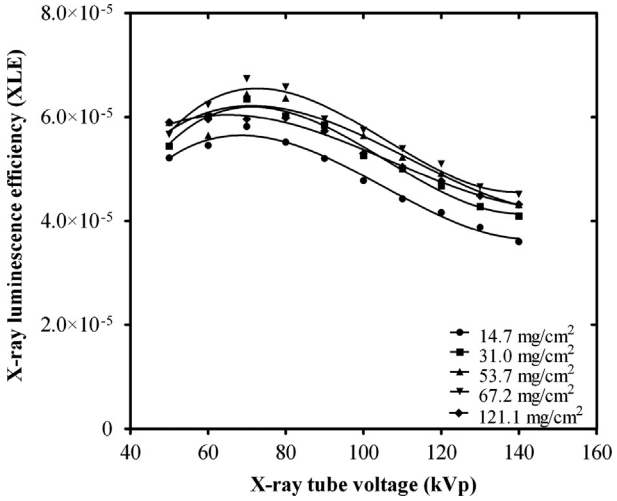

Fig. 10. Variation of the X-ray luminescence efficiency (XLE) of $GdAlO_3$:Ce scintillators for radiography X-ray tube voltages, between 50 and 140 kVp.

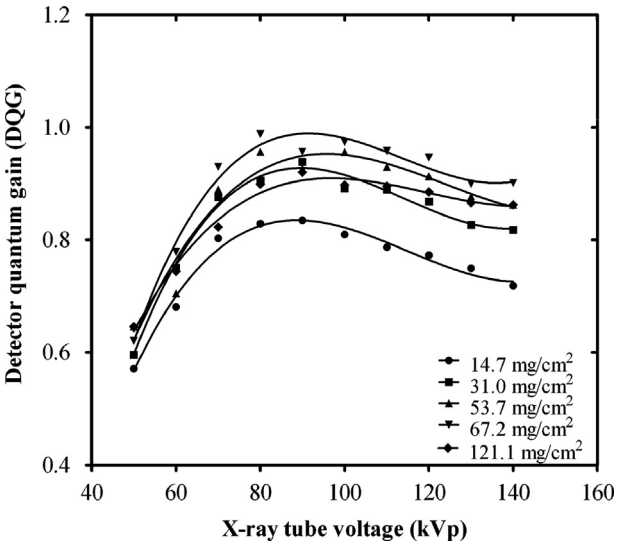

Fig. 11. Variation of detector quantum gain (DQG) of $GdAlO_3$:Ce scintillators for radiography X-ray tube voltages, between 40 and 140 kVp.

output. Light is thus more easily transmitted through the phosphor grains. On the other hand low energy X-rays do not penetrate deeply within the scintillator mass. Hence light photons, which are mainly created very close to the input screen surface, are forced to travel long trajectories to escape the rear surface of the screen. This increases light attenuation (self absorption) within scintillator mass.

The DQG values of the $GdAlO_3$:Ce phosphor screens are shown in Fig. 11. The shape of the DQG curves may be explained by considering the combined effects of: (1) The increasing number of optical photons created per absorbed X-ray, which increases DQG with X-ray energy and correspondingly affects the variation of DQG. (2) The X-ray absorption which, decreases with increasing tube voltages and affects DQG in a similar way. This is more evident in the high energy part of the curve. In addition, it is observed that DQG increases with increasing coating thickness. In the 50 to 80 kVp X-ray tube voltage range, DQG values, increase up to a maximum value and decrease thereafter.

The optimum theoretical fit to the experimental *AE* values was found for $\sigma = 67\ cm^2/g$ and η_c equal to 0.0009. This σ value is considered high, although it is lower than the values reported for other Ce doped phosphors (i.e. YAP:Ce having a $\sigma = 104\ cm^2/g$).

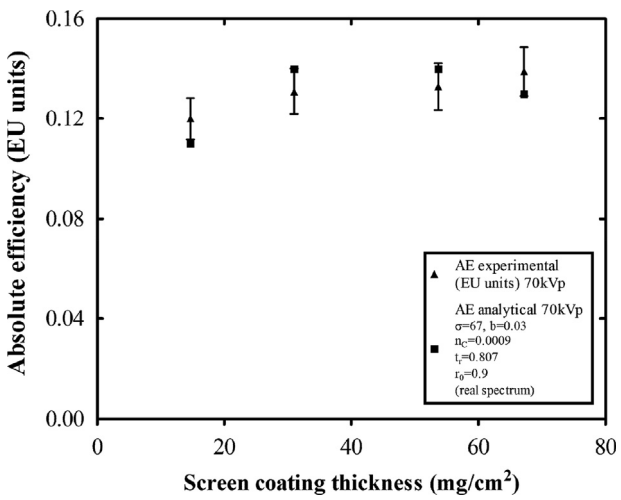

Fig. 12. Comparison between the experimental and theoretical absolute efficiency values for various screen thicknesses of the $GdAlO_3$:Ce powder screens.

However, it is higher than values reported for Eu or Tb activated phosphors [5,38]. The corresponding η_c value is among the lowest ever reported for any phosphor material and corresponds to a low light yield. For the $GdAlO_3$:Ce scintillator, light yield values, ranging from 840 photons/MeV to 9000 photons/MeV, have been reported under X-ray excitation, depending upon Ce concentration in single crystal form scintillators [18]. These values correspond to η_c in the range from 0.03 to 0.35, assuming that the optical photon energy equals to 3.875 eV. The calculated η_c value of this work corresponds to an approximate light yield of 232 optical photons per MeV. However under consideration should be taken that the 232 optical photons per MeV correspond to the presented scintillating screens prepared by granular phosphors and not to the single crystal scintillators reported [18]. The rather high σ value, in conjunction with the low η_c is in agreement with the previous discussion with regards to the small efficiency of the Ce^{3+} emission. Fig. 12 shows a comparison between the experimental and theoretical absolute efficiency values for various screen thicknesses at the 70 kVp X-ray spectrum.

The difference between theoretical and experimental AE values is below 0.01. This may be partially attributed to the experimental error in the AE measurements, shown in Fig. 12, which was calculated as 7% [41]. In addition the theoretical model presents limited accuracy in thin screens (i.e. the 14.7 mg/cm^2 $GdAlO_3$:Ce screen), where the points of X-ray interactions are close to the phosphor output [23]. However the values of the optical parameters used in calculation of 2.11 and 2.12 have been chosen considering the thin screen performance in an effort to demonstrate the effect of screen thickness on the $GdAlO_3$:Ce efficiency.

4. Conclusion

In the present study, the quantum detection efficiency (QDE), the energy absorption efficiency (EAE), the X-ray luminescence efficiency and the spectral compatibility of five $GdAlO_3$:Ce powder scintillator screens, were investigated under conditions usually met in X-ray imaging conditions. Furthermore intrinsic parameters of these screens were evaluated by using analytical modeling. The X-ray quantum detection efficiency and energy absorption efficiency were found higher than currently employed materials (e.g. aluminum perovskite ($YAlO_3$:Ce) also known as YAP:Ce) for detection of X-rays. Peak absolute efficiency was obtained for the 67.2 mg/cm^2 screen at X-ray tube voltages from 100 to 120 kVp. However, absolute luminescence efficiency maintains low values,

within the energy range under consideration compared to $YAlO_3$:Ce. The emission spectrum of $GdAlO_3$:Ce screen showed good spectral compatibility with currently used detectors (mainly analogue).

Acknowledgments

This research has been co-funded by the European Union (European Social Fund) and Greek national resources under the framework of the "Archimedes III: Funding of Research Groups in TEI of Athens" project of the "Education & Lifelong Learning" Operational Programme.

References

[1] J.M. Boone, Handbook of medical imaging, in: J. Beutel, H.L. Kundel, R.L. Van Metter (Eds.), Physics and Psycophysics, vol. 1, SPIE Press, Bellingham, 2000, pp. 36–57.
[2] G.G. Blasse, B.C. Grabmaier, Luminescent Materials, Springer-Verlag, Berlin, Heidelberg, 1994.
[3] C.W.E. van Eijk, Phys. Med. Biol. 47 (2002) 85.
[4] P. Dorenbos, Phys. Rev. B: Condens. Matter 65 (2002) 235110.
[5] N. Kalivas, I. Valais, D. Nikolopoulos, A. Konstantinidis, A. Gaitanis, D. Cavouras, C.D. Nomicos, G. Panayiotakis, I. kandarakis, Appl. Phys. A 89 (2007) 443.
[6] N. Kalivas, I. Valais, G. Salemis, C. Karagiannis, A. Konstantinidis, D. Nikolopoulos, G. Loudos, N. Sakelios, N. Karakatsanis, K. Nikita, V.L. Gayshan, I. Sianoudis, N. Giokaris, C.D. Nomicos, N. Dimitropoulos, A.V. Gektin, D. Cavouras, G. Panayiotakis, I. Kandarakis, Nucl. Instr. Meth. A 569 (2006) 210.
[7] A. Toutountzis, C. Michail, I. Valais, S. David, G. Nikiforidis, I. Kandarakis, e-J. Sci. Technol. 4 (3) (2009) 23.
[8] S.A. Smirnova, L.I. Kazakova, A.A. Fyodorov, M.V. Korzhik, J. Lumin. 60&61 (1994) 960.
[9] D.C. Cook, J.D. Cashion, J. Phys. C: Solid State Phys. 13 (1980) 4199.
[10] Y.H. Han, M. Nagata, N. Uekawa, K Kakegawa, Br. Ceram. Trans. 103 (5) (2004) 219.
[11] E. Van Der Kolk, P. Dorenbos, J.T.M. De Haas, C.W.E. Van Eijk, Phys. Rev. B: Condens. Matter 71 (2005) 045121.
[12] L. Lan, X. Zhihuang, Z. Naigen, J. Rare Earths 28 (2010) 91.
[13] M.J. Weber, Handbook of Optical Materials, CRC Press, Boca Raton, Florida, USA, 2003.
[14] J.W.M. Verweij, M.Th. Cohen-Adad, D. Bouttet, H. Lautesse, B. Moine, C. Predini, Chem. Phys. Lett. 239 (1995) 51.
[15] M. Nikl, K. Nitsch, E. Mihokova, N. Solovieva, J.A. Mares, P. Fabeni, G.P. Pazzi, M. Martini, A. Vedda, S. Baccaro, Appl. Phys. Lett. 77 (2000) 2159.
[16] I. Toshinori, O. Mamoru, U. Satoshi, S. Tsuguo, H. Toshio, Sci. Technol. Adv. Mater. 3 (2002) 239.
[17] P. Dorenbos, J. Non-Cryst. Solids 324 (2003) 220.
[18] P. Dorenbos, E. Bougrine, J.T.M. deHaas, C.W.E. van Eijk, M.V. Korzhik, Radiat. Eff. Defects Solids 135 (1995) 819.
[19] C. Adelmann, J. Swerts, S. Van Elshocht, J. Kittl, European Patent Application EP 2 337 064 A2.
[20] M. Atsuyuki, S. Shin-ichi, F. Itsuhiro, European Patent Application, EP 1 811 580 A1, 2007.
[21] K. Nakata, M. Endo, K. Doguchi, S. Fujino, US Patent US 2010/0081561 A1, 2010.
[22] S. Cizauskaite, G. Spakauskaite, A. Beganskiene, A. Kareiva, Chemija 17 (4) (2006) 40.
[23] C.M. Michail, V.A. Spyropoulou, G.P. Fountos, N.E. Kalyvas, I.G. Valais, I. S. Kandarakis, G.S. Panayiotakis, IEEE Trans. Nucl. Sci. 58 (1) (2011) 314.
[24] R.D. Evans, The Atomic Nucleus, McGraw-Hill, New York, 1955.
[25] J.A. Seibert, J.M. Boone, J. Nucl. Med. Technol. 33 (2005) 3.
[26] C.M. Michail, I.G. Valais, A.E. Toutountzis, N.E. Kalyvas, G.P. Fountos, S.L. David, I.S. Kandarakis, G.S. Panayiotakis, IEEE Trans. Nucl. Sci. 55 (6) (2008) 3703.
[27] J.H. Hubbell, S.M. Seltzer, NISTIR 5632 (1995).
[28] E. Storm, H. Israel, Report LA-3753, Los Alamos Scientific Laboratory, University of California, CA, 1967.
[29] J.A. Mares, M. Nikl, C. Pedrini, D. Bouttet, C. Dujardin, B. Moine, J.W.M. Verweij, J. Kvape, Radiat. Eff. Defects Solids 135 (1995) 369.
[30] J.R. Greening, Fundamentals of Radiation Dosimetry, IOP, London, 1985.
[31] S. Coh, Electronic Structure Theory: Applications and Geometrical Aspects, Ph.D. Thesis, Rutgers University, 2011.
[32] C. Michail, A. Toutountzis, S. David, N. Kalivas, I. Valais, I. Kandarakis, G. S. Panayiotakis, Appl. Phys. B 95 (2009) 131.
[33] C.M. Michail, G.P. Fountos, S.L. David, I.G. Valais, A.E. Toutountzis, N.E. Kalyvas, I.S. Kandarakis, G.S. Panayiotakis, Meas. Sci. Technol. 20 (2009) 104008.
[34] C.M. Michail, Investigation of Optical and Imaging Characteristics of Fluorescent Screens for Use in Digital Imaging Detectors Suitable for Telemedicine, Ph.D. Thesis, University of Patras, Greece, 2010.
[35] Oriel 70451 Integrating Sphere data sheet, Oriel Instruments, Internet site address: ⟨http:/www.spectraphysics.com/com/cda/products/all_products/0,1061,101188%2000,00/⟩.
[36] I.G. Valais, C.M. Michail, S.L. David, A. Konstantinidis, D.A. Cavouras, I. S. Kandarakis, G.S. Panayiotakis, IEEE Trans. Nucl. Sci. 55 (2) (2008) 785.
[37] C.M. Michail, G.P. Fountos, P.F. Liaparinos, N.E. Kalyvas, I. Valais, I.S. Kandarakis, G.S. Panayiotakis, Med. Phys. 37 (7) (2010) 3694.
[38] I. Kandarakis, D. Cavouras, G. Panayiotakis, T. Agelis, C. Nomicos, G. Giakoumakis, Phys. Med. Biol. 41 (1996) 297.
[39] Del Mar Ventures (2007), ⟨http:/www.sciner.com/Opticsland/FS.htm⟩.
[40] C.M. Michail, G.P. Fountos, I.G. Valais, N. Kalyvas, P. Liaparinos, I.S. Kandarakis, G.S. Panayiotakis, IEEE Trans. Nucl. Sci. 58 (5) (2011) 2503.
[41] D. Nikolopoulos, N. Kalyvas, I. Valais, X. Argyriou, E. Vlamakis, T. Sevvos, I. Kandarakis, J. Inst. 7 (2012) P11021.